Science Arts & Métiers (SAM)

is an open access repository that collects the work of Arts et Métiers ParisTech researchers and makes it freely available over the web where possible.

This is an author-deposited version published in: https://sam.ensam.eu
Handle ID: .http://hdl.handle.net/10985/18677

To cite this version :

Olivier CASTELNAU - Mechanical behavior of polycrystalline materials - 2011

Any correspondence concerning this service should be sent to the repository Administrator : archiveouverte@ensam.eu

Arts et Métiers Institute of Technology

MECHANICAL BEHAVIOR OF POLYCRYSTALLINE MATERIALS

O. Castelnau

Laboratoire Procédés et Ingénierie en Mécanique et Matériaux,
CNRS UMR8006, Arts & Métiers ParisTech
151 Bd de l'hopital, 75013 Paris, France
Email: olivier.castelnau@paris.ensam.fr

1 Introduction

From the mechanical point of view, polycrystalline materials have to be considered as a specific class of composites. They are composed of many grains, with grains size ranging from nm to cm scales. Grains are generally assembled in a random way, *i.e.* their size, shape, and lattice orientation do not depend on the size, shape, and orientation of the surrounding grains (figure 1). Therefore, the microstructure of polycrystals can hardly be described exactly. Most of the time, one can only access a statistical characterization of grain arrangement *e.g.* with the help of cross-correlation functions. In the Euler orientation space, microstructure description is generally limited to the distribution of crystal lattice orientations (Orientation Distribution Function, ODF, or crystallographic texture).

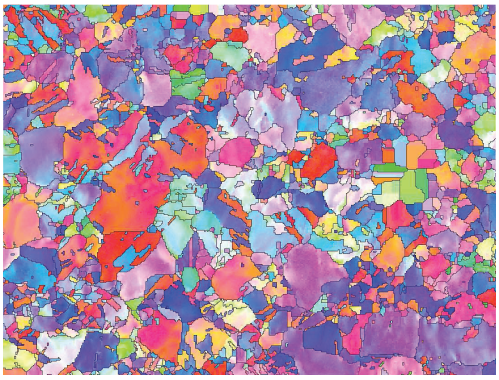

Figure 1: Typical 2D microstructure of a copper polycrystal, imaged by the Electron Back Scattered Diffraction (EBSD) technique. Average grain size is $\sim 10\mu\,\mathrm{m}$.

The complex behavior of polycrystalline materials comes from the anisotropic behavior at the grain scale, closely related to the symmetry of the crystal lattice. This is true for all quantities of interest here, such as elasticity, (visco)plasticity, thermal dilatation, ... Grains exhibiting different lattice orientations react differently to a given stress level. As far as grain boundaries maintain the cohesion of the material, the *local* stress (*i.e.* inside a grain) differs from the *overall* one (the applied stress), leading to a heterogeneous distribution of stress and strain fields within the polycrystal.
Most research efforts in the past years have been focussed on the understanding of the build-up of these heterogeneities, in relation with the microstructure and local (grain) behavior, since they greatly influence the overall behavior. For instance, plasticity in a polycrystal can start far below the macroscopic yield stress; it is sufficient that the local stress reaches the local yield stress somewhere in the structure where stress concentration is large enough such as along grain boundaries [1].

In this chapter, we review (not in an exhaustive way) some experimental, numerical, and theoretical techniques used for the investigation of the mechanical behavior of polycrystalline materials. We mostly focus on materials exhibiting micrometric grain size, so that continuum mechanics still applies. At smaller (*e.g.* nanometric) grain size, the volume of grains boundaries becomes non-negligeable compared to the volume of grains, and thus their specific behavior should be taken into account; this point will however not be treated here.

2 Experimental characterization of mechanical fields in polycrystals

There has been quite a number of experimental developments during the last decade as for the experimental characterization of strain and stress fields in deformed polycrystals, at an intragranular scale. A sufficiently large number of adjacent grains (denoted the Representative Volume Element – RVE) must be scanned simultaneously to capture the overall material behavior. The complex localization of strain and stress within specific (part of) grains needs to be described in connection with the local material microstructure and grain mechanical behavior.

2.1 Displacement and strain fields

The analysis of intragranular strain field in polycrystalline material exhibiting micrometric grain size has been significantly developed since $\sim$ a decade. In fact the local total strain cannot be measured directly. One has to measure the displacement field over the Region Of Interest (ROI), and to evaluate the derivative of this displacement to get the strain field. This derivative is evaluated for a given gage length, *e.g.* by a finite difference scheme or with more advanced techniques [2], and therefore the strain that can be estimated is not exactly a local value but the mean value over the length used for the derivative. Consequently, strain localization is necessarily smeared out with this technique, just as for standard strain gages.
Displacement field can be obtained with very good accuracy by Speckle interferometry, *e.g.* [3]. Due to the interference of two in-phase laser beams, the specimen surface roughness creates a Speckle pattern that is recorded by a camera. Strain field can be obtained from the modification of this pattern as the specimen is deformed. Displacement resolution can be as good as $20 - 30\mathrm{n\,m}$ but spatial resolution is limited to a few micrometer due to the diffraction in the camera optics. For in situ deformed specimen, strain increments must be very small to recover the complete strain history.
A good compromise between ease of use, simplicity of sample preparation, displacement accuracy, and spatial resolution is obtained by Digital Image Correlation (DIC), *e.g.* see [4, 5] The method consists in taking successive images of the same ROI as the specimen is deformed. Then, small sub-images (which size is typically 15×15pixels) of the initial image are selected, and their position is found back in the deformed image, for exemple by maximizing the correlation coefficient between both sub-images. Subpixel accuracy of DIC, which can reach few hundredths of pixels, is obtained by an interpolation of gray level allowing subpixel shift and small distorsion of the subimage (rotation, deformation) necessary to obtain the best match between both subimages. Since the accuracy of DIC is directly correlated with the gray level gradient of the sub-image, it is often necessary to apply a speckle pattern on the specimen surface, *e.g.* by projecting black droplets on the white painted surface when millimetric spatial resolution is enough, or by pulverisation of thin metallic dots or lines (*e.g.* Au) by microlithography for micrometric resolution. In the last case, image of the specimen surface can be obtained under Scanning Electron Microscopy. Note that this DIC method can also be combined with tomography techniques under synchrotron radiation in order to get 3D displacement fields [4, 6].
Exemple of results obtained by DIC is given in figure 2 in a specimen of ice deformed plastically under creep. The specimen microstructure has been elaborated specifically so that grain boundaries (columnar microstructure) and the only available slip plane for dislocations lie perpendicular to the specimen observation surface. Therefore,

the plastic deformation is essentially 2D and no in-thickness displacement gradient is expected. It can be observed that strain is highly localized into bands extending over several grain sizes, and local strain can reach values as large as 10 times the macroscopic one. Similar results have been reported for other materials, *e.g.* see [7, 8, 9]. Here, the significant intra- and inter-granular strain localization has to be associated with the huge viscoplastic anisotropy at the grain scale. Figure 2b provides a quantitative microstructure analysis, *i.e.* the Schmid factor for the slip plane (note that there is in ice no privileged slip direction in the slip plane). It can be easily observed that, contrarily to intuitive models such as the uniform stress bound (static / Reuss model), large Schmid factors are not always associated to large strains. There are many grains with large Schmid factor (thus expected to be "soft" grains) that in fact deform less than grains with small factor (expected to be "hard"). This feature is associated with the tremendous effect of intergranular mechanical interactions: the deformation of a specific grain is highly influence by the orientation and behavior of its surrounding.

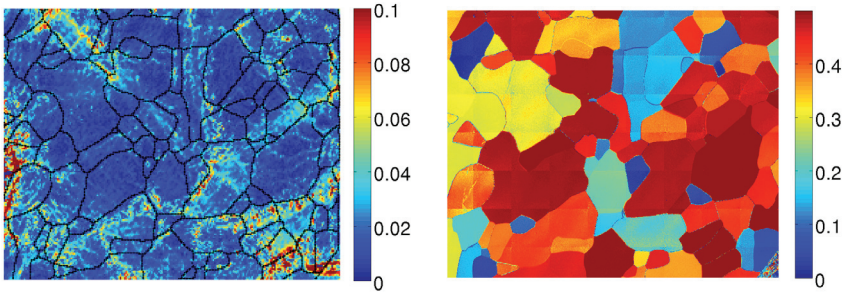

Figure 2: (left) Distribution of equivalent strain measured by DIC in a specimen of columnar ice deformed by creep under uniaxial compression. Grain boundaries are indicated in black. (right) Map of corresponding Schmid factor for the basal slip system. Grain size is centimetric. Overall deformation is $\sim 1\%$. From [10]

2.2 Stress field

The stress field in polycrystalline materials cannot be measured directly. Instead, one can measure the *elastic* strain related to the applied or residual stress, and make use of Hooke's law to calculate the stress. Elastic strain can be efficiently measured at different scales by diffraction techniques, but we will see that going from the measured elastic strain to the desired stress is not always an easy task; this step generally requires having estimated the 6 components of the elastic strain tensor for the ROI.

2.2.1 From diffraction data to strain distribution The elastic strain (distribution) can be best measured by diffraction techniques [11]. Let consider an incident parallel and monochromatic beam which wavelength λ is of the order of magnitude of interatomic distances of the specimen. The beam, that can be composed of electrons, neutrons, or photons (X-rays from laboratory or synchrotron sources), interacts with the specimen and is diffracted in different directions. The diffraction volume (denoted Ω) can range from few hundreds of $\mathrm{n\,m}^3$ for electron diffraction up to $\sim \mathrm{c\,m}^3$ for neutrons. Penetration depth of the beam also ranges from $\mathrm{n\,m}$ to $\sim \mathrm{c\,m}$ depending on the kind of radiation used. There are therefore a large spectrum of possible experimental setup, leading to analyses at different scales.
We denote $\mathbf{k}_i$ and $\mathbf{k}_d$ the incident and diffracted wave vectors (their norm is $k_i = k_d = 1/\lambda$) respectively. When the beam hits a large single grain that does not contain lattice

defects (*i.e.* a perfect crystal), the intensity of the outgoing beam has non-vanishing value only for very specific directions $\theta = \theta_B$ (2θ is the angle between incident and diffracted beams) given by Bragg's law

$$\frac{1}{d_{hkl}} = \frac{2\sin\theta_B}{\lambda} \tag{1}$$

with d_{hkl} the distance between lattice planes of Miller indices $\{hkl\}$ and θ_B the Bragg angle. This property can also be written $\mathbf{g} = \mathbf{K}$ with $\mathbf{g}$ the reciprocal lattice vector (its norm is $g = 1/d_{hkl}$) of the considered crystal and $\mathbf{K} = \mathbf{k}_d - \mathbf{k}_i$ the diffraction vector. In other words, introducing vector $\mathbf{s}$ such that $\mathbf{K} = \mathbf{g} + \mathbf{s}$, the intensity diffracted by a large and perfect crystal vanishes unless the diffraction vector corresponds to $\mathbf{s} = \mathbf{0}$ (figure 3).

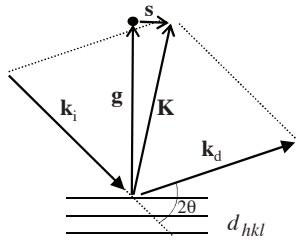

Figure 3: Reciprocal lattice vector $\mathbf{g}$ corresponding to the lattice plane (hkl), and diffraction vector $\mathbf{K}$. For perfect and large crystals, diffraction occurs only for $\mathbf{K} = \mathbf{g}$.

However, for heterogeneously deformed materials of interest here, Bragg's law does not strictly applies. Individual grains generally contain a large density of lattice defects (such as dislocations), and lattice plane distances vary between grains but also inside individual grains due to the heterogeneous stress field. Let $\mathbf{u}(\mathbf{x})$ be the displacement field inside the material, measured from the initial stress free configuration. The diffracted intensity has a non-zero value in the vicinity of reciprocal lattice nodes $\mathbf{g}$. Considering intensity distribution in the direction $\mathbf{K} \parallel \mathbf{g}$, the Fourier transform $\hat{I}(n)$ of the diffracted intensity $I(s)$ reads

$$\hat{I}(n) = I_0 \langle \exp(2\pi K n i \bar{\varepsilon}_{\mathbf{K},n}) \rangle_\Omega \tag{2}$$

where $\langle . \rangle_\Omega$ denotes the volume average over the diffraction volume Ω, and i the imaginary unit. Here, n corresponds to a physical distance in the material (typically a few tens of nm) in the investigated direction (*i.e.* parallel to $\mathbf{K}$), and $\bar{\varepsilon}_{\mathbf{K},n}(\mathbf{x})$ is the mean elastic strain at a position $\mathbf{x}$, in direction $\mathbf{K}$, and averaged over a distance n

$$\bar{\varepsilon}_{\mathbf{K},n}(\mathbf{x}) = \frac{\Delta\mathbf{u}.\mathbf{K}}{nK} \tag{3}$$

with $\Delta\mathbf{u}$ the relative displacement between two atoms separated by a vector $\mathbf{n}$. It can be noted that the (real) axial elastic strain $\varepsilon_{KK}(\mathbf{x})$ in direction $\mathbf{K}$, usually called "lattice strain", is simply the limit of $\bar{\varepsilon}_{\mathbf{K},n}(\mathbf{x})$ as the gage length tends to 0

$$\varepsilon_{KK}(\mathbf{x}) = \frac{1}{K^2}\mathbf{K}.\boldsymbol{\varepsilon}.\mathbf{K} = \lim_{n\to 0} \bar{\varepsilon}_{\mathbf{K},n}(\mathbf{x}) \; . \tag{4}$$

Interestingly, the distribution of ε_{KK} can be determined from the diffracted intensity. Corresponding relations can be obtained by using the standard property relating the successive derivatives of $\hat{I}(n)$ at $n = 0$ with the moments $\mu^{(m)}[I(s)] = \int s^m I(s) ds$ of degree m of $I(s)$. They read

$$\langle \varepsilon_{KK} \rangle_\Omega = -\frac{1}{K} \frac{\mu^{(1)}}{\mu^{(0)}} , \qquad \langle \varepsilon_{KK}^2 \rangle_\Omega = \frac{1}{K^2} \frac{\mu^{(2)}}{\mu^{(0)}} . \tag{5}$$

Moments of the (directional) elastic strain can thus be estimated accurately. One must however keep in mind that optical abberations associated with the diffractometer setup have to be considered for proper quantitative analyses, in particular when high order ($m \geq 2$) moments are of interest [12].
Diffraction analyses can thus be considered as field measurements, with two setup of particular interest for micromechanical studies. (i) When the gage volume is smaller than the grain size, spatial heterogeneities of elastic strain can be mapped. (ii) When gage volumes have similar size than the RVE, spatial resolution is lost but heterogeneities of the average strain field can be mapped in the orientation (Euler) space.

2.2.2 Stress field in the cartesian space Stress field in the cartesian space can be obtained if the beam cross section and penetration depth is smaller than the grain size. There are different possible setup for this:

- One solution consists in focussing a polychromatic X-ray beam down to (sub)micrometric cross section by means of a pair of mirrors (Kirkpatrick-Baez optic). This focussed beam hits part of a single grain in the polycrystal, and the so-generated Laue diffraction pattern is recorded by a 2D detector. Dedicated setup are available at synchrotron facilities such as ESRF (France), APS, or ALS (USA). Exemple of results are shown in figure 4. Since the shape of Laue pattern is closely related to that of the crystal lattice, local elastic strain can be identified [13].

- A second solution is based on the precise analysis of Kikuchi pattern formed by the back scattered electrons in a Scanning Electron Microscope (SEM). As for Laue, the geometry of Kikuchi pattern can reveal lattice distorsion with high accuracy. Example of applications of this high-Resolution EBSD technique can be found application in [14, 15, 16].

- Another solution consists in using Kossel patterns formed in a SEM when the energy of the incident electron beam energy is large enough. The diffuse X-ray source generated in the specimen diffracts within the grain [17]. Fluorescence radiation is also generated at the same time, limiting thus the signal-to-noise ratio to values close to 1.

2.2.3 Stress field in the orientation space Stress field in the Euler space can be advantageously characterized by means of highly penetrating radiation, such as neutrons or very hard X-rays for which the penetration depth far exceed standard grain sizes. If the beam cross section is large enough, the mechanical response of a whole RVE can be investigated.
For the analysis of data, one of the issues is related to the identification of the source of the measured elastic strain. For macro-homogeneous materials (no microstructure nor composition gradient in the investigated volume), there are basically two sources of strain:

1. The uniform stress $\bar{\boldsymbol{\sigma}}$ applied at the specimen surface generates a heterogeneous stress field $\boldsymbol{\sigma}(\mathbf{x})$, and the associated field of elastic strain $\boldsymbol{\varepsilon}(\mathbf{x})$. Here, $\bar{\boldsymbol{\sigma}}$ is the volume average of local stresses, $\bar{\boldsymbol{\sigma}} = \langle \boldsymbol{\sigma} \rangle$.

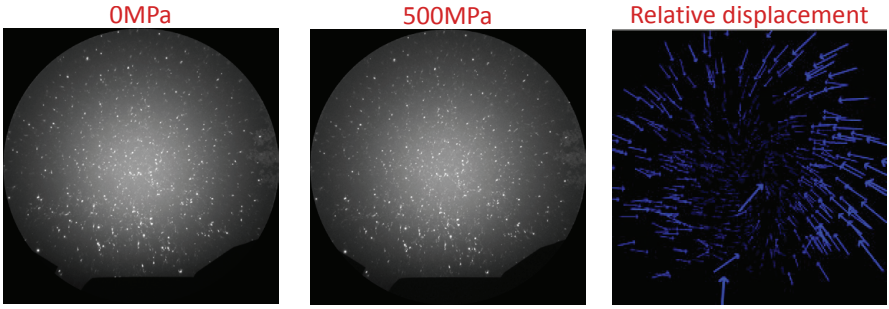

Figure 4: Modification of the Laue pattern of an individual grain of a tungsten polycrystal (grain size $\sim 5\mu\,\mathrm{m}$) deformed in situ. (left) Pattern at the initial state, *i.e.* for $\bar{\boldsymbol{\sigma}} = 0\mathrm{MPa}$, (center) for $\bar{\boldsymbol{\sigma}} = 500\mathrm{MPa}$, and (right) relative motion of Laue spots on the detector between initial and deformed configurations, determined by image processing (arrows are enlarged by a factor 50). Data obtained at beamline BM32 of the ESRF.

2. Upon complete unloading of the specimen ($\bar{\boldsymbol{\sigma}} = \mathbf{0}$), *local* stresses do not vanish. The field of residual stress $\boldsymbol{\sigma}_{\mathrm{res}}$ is such that $\langle \boldsymbol{\sigma}_{\mathrm{res}} \rangle = \mathbf{0}$.

The local stress at any physical point $(\mathbf{x})$ thus reads

$$\boldsymbol{\sigma}(\mathbf{x}) = \mathbf{B}(\mathbf{x}) : \bar{\boldsymbol{\sigma}} + \boldsymbol{\sigma}_{\mathrm{res}}(\mathbf{x}), \tag{6}$$

with $\mathbf{B}$ the stress localization tensor of the purely elastic problem. The combination of (4), (6), and Hooke's law gives the general expression for the lattice strain [18, 19]

$$\langle \varepsilon_{KK} \rangle_\Omega = \frac{\mathbf{K} \otimes \mathbf{K}}{K^2} \langle \mathbf{S} : \mathbf{B} \rangle_\Omega : \bar{\boldsymbol{\sigma}} + \langle \mathbf{S} : \boldsymbol{\sigma}_{\mathrm{res}} \rangle_\Omega \tag{7}$$

with $\mathbf{S}$ the elastic compliance of grains. In metallurgy, X-ray diffraction is often used for "stress analysis", *i.e.* the overall stress $\bar{\boldsymbol{\sigma}}$ is determined from the measurement of many lattice strain $\langle \varepsilon_{KK} \rangle_\Omega$ in different directions. From (7), it can be seen that this is possible only when $\langle \mathbf{S} : \boldsymbol{\sigma}_{\mathrm{res}} \rangle_\Omega$ can be neglected, which is not always a reasonable assumption. For example, after plastic deformation, it has been shown that intragranular stress heterogeneity in zirconium alloys is $\sim 100\mathrm{MPa}$, *i.e.* of the same order of magnitude than the macroscopic yield stress [20]. In that case, the determination of $\bar{\boldsymbol{\sigma}}$ is inaccurate unless the precise distribution of $\boldsymbol{\sigma}_{\mathrm{res}}$ (in that case due to plasticity) is known.
The "$\sin^2 \psi$ law" generally used for stress analyses, and implemented in most commercial softwares as a standard method, can be obtained from (7) when taking $\boldsymbol{\sigma}_{\mathrm{res}}(\mathbf{x}) = \mathbf{0}\ \forall \mathbf{x}$ and isotropic elastic properties at the grain scale (leading to $\mathbf{B} = \mathbf{I}$). Unfortunately it is not uncommon to see in the literature applications of this method to cases for which these conditions are not met.

3 Modeling

We discuss now actual possibilities to reach, to estimate, or to bound the mechanical behavior of polycrystalline aggregates by means of theoretical or numerical models. We consider polycrystals exhibiting a stationary microstructure (*e.g.* no microstructure gradient at the scale of a RVE) and submitted to homogeneous boundary conditions. There are basically two strategies to get the mechanical response: mean-field

and full-field approaches. For both of them, the key issue is the estimation of the stress or strain localization tensors, in relation with the microstructure and local behavior of grains. Basically, the problem to be solved is to find an equilibrated stress field, related to a compatible strain field with the local constitutive relation, both fields fulfilling the applied boundary conditions. Once localization tensors are known, the most difficult part of the problem is solved.

3.1 Full-field modeling

The goal of full-field approaches is to find complete stress and strain fields within the polycrystal. The polycrystal is meshed with a mesh size smaller than the grain size in order to capture intragranular strain heterogeneities, and the problem is then solved numerically. Stress concentration next to grain boundaries, or the mechanical interaction between two specific grains, can thus be investigated. The main advantage of this approach is the generation of an "exact" (within numerical inaccuracies) solution for the problem. However, there are basically three difficulties to overcome.
As detailed previously, polycystal microstructures are complex since they exhibit specific random features. On the other hand, the use of full-field approaches requires the precise knowledge of the microstructure to be meshed and solved. There are two strategies to deal with this issue. (i) When the specimen is adapted (a small sample comprising a small number of poorly deformed grains, random crystallographic texture, ...), the exact 2-D microstructure can be measured *e.g.* by diffraction and contrast X-ray tomography [21]. Grains can then be meshed explicitly and the problem solved. (ii) But most of the time, the above conditions are not met, and the microstructure to be solved numerically has to be guessed. There are many models in the literature as for the generation of random microstructures exhibiting specific statistical properties [22]. As noted by [23], simple Voronoi tesselations are not well adapted owing to a limited grain size distribution compared to standard real microstructures.
To get the effective behavior of a polycrystalline material, the microstructucture to be solved should be of size equal or larger than the RVE size. Although RVE size can be adjusted depending on the desired result accuracy, it usually comprises too many grains so that the associated numerical full-field problem cannot be solved at once with standard computer capacities. This issue can be solved assuming ergodicity. In that case, volume average can be substitute by ensemble average. This means that the solution can be obtained by solving numerically many random microstructures, each of size smaller than the RVE, and then performing ensemble averages over all of these smaller microstructures [24]. The number of "small" microstructures can be determined depending to the desired result accuracy, the kind of result of interest (effective behavior, or stress/strain distributions, etc...), and the size of these microstructures. With actual computer capacities, it is generally of the order of a few tens.
As for the numerical scheme to be used for solving microstructures, although calculations are possible using the Finite Element Method [24, 25, 26, 27], a numerically more efficient method based on Fast Fourier Transforms (FFT) has been proposed recently [28, 29], and applied to polycrystals [30]. The method is limited to periodic microstructures and, unlike FEM, it can solved the case of incompressible behavior as well as composites exhibiting an infinite mechanical contrast between the phases (such as composites with rigid inclusions). Briefly, the method is based on the fact that the local mechanical response of a periodic heterogeneous medium can be calculated as a convolution integral between the Green function of a linear reference homogeneous medium and a polarization field. Since such integrals reduce to a simple products in the Fourier space, efficient Fast Fourier Transform algorithms can be used to transform the heterogeneity field into the Fourier space and, in turn, get the mechanical fields by transforming that product back to real space. An iterative scheme must be implemented to obtain, upon convergence, a compatible strain field and a stress field in equilibrium, see [29, 31] for details. Recent comparisons between FEM and FFT performance and results can be found in [32].

3.2 Mean-field modeling

3.2.1 Linear thermo-elasticity In fact, it is not necessary to know the full field of localization tensors in order to get the effective behavior of polycrystalline materials. For reasons that will become evident in the sequel, let us consider the case of thermo-elastic polycrystals. Local and effective constitutive relations read respectively

$$\boldsymbol{\varepsilon}(\mathbf{x}) = \mathbf{S}(\mathbf{x}) : \boldsymbol{\sigma}(\mathbf{x}) + \boldsymbol{\varepsilon}_0(\mathbf{x}), \qquad \bar{\boldsymbol{\varepsilon}} = \tilde{\mathbf{S}} : \bar{\boldsymbol{\sigma}} + \tilde{\boldsymbol{\varepsilon}}_0 \ , \tag{8}$$

with $\boldsymbol{\varepsilon}_0$ a thermal strain occurring stress free due to temperature changes. Symbols $\tilde{.}$ and $\bar{.} = \langle . \rangle$ denote the homogenized (or effective) property and the volume average over the whole polycrystal volume, respectively. It can be shown that the effective stiffness $\tilde{\mathbf{S}}$ and the effective thermal strain $\tilde{\boldsymbol{\varepsilon}}_0$ read

$$\tilde{\mathbf{S}} = \langle \mathbf{S}(\mathbf{x}) : \mathbf{B}(\mathbf{x}) \rangle, \quad \tilde{\boldsymbol{\varepsilon}}_0 = \langle \boldsymbol{\varepsilon}_0(\mathbf{x}) : \mathbf{B}(\mathbf{x}) \rangle \ . \tag{9}$$

Since, for thermo-elastic polycrystals, the elastic compliance and the thermal dilatation are uniform properties inside grains, the quantities $\mathbf{S}(\mathbf{x})$ and $\boldsymbol{\varepsilon}_0(\mathbf{x})$ in equation (8a) can be replaced by the corresponding homogeneous values $\mathbf{S}^{(r)}$ and $\boldsymbol{\varepsilon}_0^{(r)}$ of the considered phase (r). Similar substitution can be made in equation (9) leading to

$$\tilde{\mathbf{S}} = \sum_r c^{(r)} \mathbf{S}^{(r)} : \mathbf{B}^{(r)} \ , \quad \tilde{\boldsymbol{\varepsilon}}_0 = \sum_r c^{(r)} \boldsymbol{\varepsilon}_0^{(r)} : \mathbf{B}^{(r)} \tag{10}$$

with $.^{(r)}$ indicating the average over the volume of phase (r), *e.g.* $\mathbf{B}^{(r)} = \langle \mathbf{B}(\mathbf{x}) \rangle_{(r)}$, and $c^{(r)}$ the volume fraction of phase (r). Here, a *mechanical phase* (r) denotes the set of all grains of the polycrystal having the same crystal orientation; those grains have different shape and environment but their elastic and thermal properties are identical. From (10), it can be observed that the sole knowledge of the mean (phase average) values $\mathbf{B}^{(r)}$ is sufficient to estimate the overall polycrystal behavior. It can be anticipated that, if the quantities $\mathbf{B}^{(r)}$ can be calculated without having to know the complete field of $\mathbf{B}(\mathbf{x})$, computation will be way faster. Hence the denomination of "mean-field" approaches.
With the effective behavior in hand, statistical averages over crystal orientations (r) can be estimated. Basically, two quantities can be obtained from mean-field approaches:

1. The phase average stress (or first moment) $\boldsymbol{\sigma}^{(r)}$ expresses

$$\boldsymbol{\sigma}^{(r)} = \mathbf{B}^{(r)} : \bar{\boldsymbol{\sigma}} + \boldsymbol{\sigma}_{\text{res}}^{(r)}, \tag{11}$$

   with $\boldsymbol{\sigma}_{\text{res}}^{(r)}$ the average residual stress of phase (r). The knowledge of $\boldsymbol{\sigma}^{(r)}$ for all phases (r) allows investigating the so-called *interphase* heterogeneities, *i.e.* the variation of the phase average stress with respect to the crystal orientation.

2. Deeper insight into the stress distribution can be obtained from the second moment $\langle \boldsymbol{\sigma} \otimes \boldsymbol{\sigma} \rangle^{(r)}$ of the stress ($\otimes$ denotes the dyadic product), which is simply the tensorial expression for the mean of the square of the stress. It can be obtained by a derivation of the effective energy with respect to local compliances, see [33, 34, 35, 36].

The standard deviation of the stress distribution within a given crystal orientation (r) can be estimated from these two moments as the square root of $< \boldsymbol{\sigma} \otimes \boldsymbol{\sigma} >^{(r)} - < \boldsymbol{\sigma} >^{(r)} \otimes < \boldsymbol{\sigma} >^{(r)}$; it is related to the width of the stress distribution in crystal orientation (r), and account for both the heterogeneity of stress distribution inside

grains but also the heterogeneity between grains of identical orientation but exhibiting different shapes and having different neighborhood. Similar relations can be derived for the strain statistics.
Unlike full-field approaches, mean-field methods are based on a statistical description of the microstructure of the polycrystalline aggregate. The microstructure is described by several n-points correlation functions, so that the exact position and shape of a specific grain with respect to its neighbors is not known. However, as already introduced, all grains exhibiting the same crystallographic orientation are treated as a single mechanical phase. Owing to the random character of the microstructure with all grains playing geometrically similar roles, the Self-Consistent (SC) scheme [37, 38, 39] is especially well suited for polycrystals. This model, which provides a relatively simple expression for $\mathbf{B}^{(r)}$, relies on specific microstructures exhibiting perfect disorder and infinite size graduation [40]. It is attained for example when the space is filled with spheres of different diameters until full compacity is reached. The SC scheme has often been described as if the interaction between each grain and its surrounding could be approximated by the interaction between one ellipsoidal grain with the same lattice orientation as the original grain and a homogeneous equivalent medium whose behavior represents that of the polycrystal, taking thus advantage of the analytical solution of [41] for the inclusion/matrix interaction. This reasoning led to the conclusion that the SC scheme implicitly considers uniform stress and strain-rate inside grains. This interpretation turns out to be incorrect, since intraphase stress and strain heterogeneities do not vanish as explained above, see [35] for a review.

3.2.2 Case of nonlinear behavior The mean-field estimate of *nonlinear materials* is significantly more complex than the thermo-elastic case treated above. For simplicity, let us consider the case of a viscoplastic polycrystal in which grains are deforming by glide of dislocations on specific slip planes having Miller indices $(hkl)[uvw]$, and a power-law behavior

$$\frac{\dot{\gamma}(\mathbf{x})}{\dot{\gamma}_0} = \left| \frac{\tau(\mathbf{x})}{\tau_0} \right|^{n-1} \frac{\tau(\mathbf{x})}{\tau_0} \ , \tag{12}$$

$\tau_{(k)}(\mathbf{x}) = \boldsymbol{\mu}_{(k)}^{(r)} : \boldsymbol{\sigma}(\mathbf{x})$ being the resolved shear stress acting on slip system (k), $\dot{\gamma}_{(k)}(\mathbf{x})$ the corresponding shear rate, and τ_0 and $\dot{\gamma}_0$ two constants expressing the resistance of the slip system (indices (k) and (r) have been omitted above for sake of clarity). The local strain-rate is given by a combination of shear rates

$$\dot{\boldsymbol{\varepsilon}}(\mathbf{x}) = \sum_k \boldsymbol{\mu}_{(k)}^{(r)} \dot{\gamma}_{(k)}(\mathbf{x}) \tag{13}$$

with $\boldsymbol{\mu}_{(k)}^{(r)} = \frac{1}{2}(\mathbf{n}\otimes\mathbf{b} + \mathbf{b}\otimes\mathbf{n})$ the (purely geometric) Schmid tensor depending on the orientation of the slip system, $\mathbf{n}$ and $\mathbf{b}$ being the slip plane normal and slip direction (parallel to the Burgers vector) in that plane, respectively. Obviously, the viscous compliance relating $\dot{\boldsymbol{\varepsilon}}(\mathbf{x})$ and $\boldsymbol{\sigma}(\mathbf{x})$ is not uniform within a phase, owing to the stress sensitivity $n > 1$ and the non-uniform distribution of $\boldsymbol{\sigma}$ (leading to a heterogeneous distribution of $\tau_{(k)}$) in the phase. Consequently, (9) cannot be replaced with (10).
The basic method to deal with such nonlinear behavior is to define a *Linear Comparison Polycrystal* (LCP) having the same microstructure as the real nonlinear polycrystal, and to which the linear homogenization scheme applies. Of course, the so-estimated effective behavior remains nonlinear since the definition of the LCP depends on the applied macroscopic stress. The difficult part of the problem consists of finding the best *linearization* procedure leading to the optimal selection of the LCP. Since decades, there has been quite a number of propositions in the literature dealing with this issue.
First, two very basics model can be derived, namely *static* and *Taylor* models. They are constructed by considering respectively uniform stress and uniform strain-rate

states throughout the polycrystal; they lead to vanishing intragranular stress and strain heterogeneities. These models violate strain compatibility and stress equilibrium, respectively, and are of limited accuracy when the local behavior is highly nonlinear and/or highly anisotropic, as it will be illustrate in the next section. The main interest or static and Taylor models relies on their bound character, since they provide, respectively, a lower and an upper bound for the effective stress potential. These are also the most restrictive bounds that be derived when one has not more microstructural information than just the volume fraction of the different phases. Sharper bound, such as the Hashin-Strikman ones, can be derived when additional information about the spatial repartition of the phases (here isotropy) is taken into account.

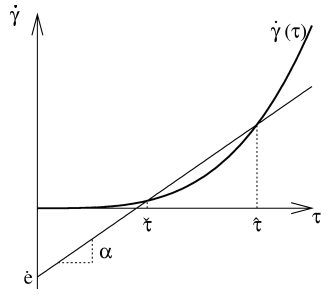

Figure 5: Schematic representation of the linearization.

More accurate estimations of the effective behavior rely on a *generalization* of the SC scheme for nonlinear behavior. The local constitutive relation given by equations (12) and (13) has to be linearized in a suitable way to obtain a form similar to (8a), with $\mathbf{S}$ and $\dot{\boldsymbol{\varepsilon}}_0$ uniform per phase (and where $\boldsymbol{\varepsilon}$ is replaced everywhere by $\dot{\boldsymbol{\varepsilon}}$). Generally speaking, the linearization can be expressed in the form depicted in figure 5 [42]

$$\dot\gamma_{(k)}(\mathbf{x}) = \alpha^{(r)}_{(k)}\tau_{(k)}(\mathbf{x}) + \dot e^{(r)}_{(k)}, \tag{14}$$

thus leading to the following expressions for $\mathbf{S}^{(r)}$ and $\dot{\boldsymbol{\varepsilon}}^{(r)}_0$

$$\mathbf{S}^{(r)} = \sum_k \alpha^{(r)}_{(k)} \boldsymbol{\mu}^{(r)}_{(k)} \otimes \boldsymbol{\mu}^{(r)}_{(k)} \ , \qquad \dot{\boldsymbol{\varepsilon}}^{(r)}_0 = \sum_k \dot e^{(r)}_{(k)} \boldsymbol{\mu}^{(r)}_{(k)} \ , \tag{15}$$

where the shear compliance $\alpha^{(r)}_{(k)}$ and stress-free shear-rate $\dot e^{(r)}_{(k)}$ can be easily expressed with respect to two reference shear stresses $\check\tau^{(r)}_{(k)}$ and $\hat\tau^{(r)}_{(k)}$, see figure 5. The optimal choice (from the point of view of the variational mechanical problem) of those reference stresses is not straightforward; this is the main reason why several extensions of the SC scheme have been proposed in the literature. Obviously, all of them reduce to the same SC model in the linear case $n = 1$.
Following [43], Masson *et al.* [44] proposed the so-called "affine" (AFF) linearization scheme which is based on the simple idea of a linear behavior (14) tangent to the nonlinear one (12) at the mean shear stress, leading to

$$\check\tau^{(r)}_{(k)} = \hat\tau^{(r)}_{(k)} = \langle \tau_{(k)} \rangle^{(r)}, \quad \alpha^{(r)}_{(k)} = \left.\frac{\partial\dot\gamma}{\partial\tau}\right|_{\tau=\check\tau^{(r)}_{(k)}} . \tag{16}$$

The main limitations of this procedure are discussed in detail in [44, 45]. One of them is the violation of rigourous upper bounds for the effective behavior. More generally,

the affine extension is known to overestimate the overall viscosity, *i.e.* to predict an effective behavior that is too stiff. This negative feature can be alleviated by means of the energy formulation originally proposed by [43] (see [46]).
Alternative, more sophisticated ways to generalize the SC scheme have been proposed by Ponte Castañeda and co-workers during the last decade. The basic idea of these methods is to guide the choice of the properties of the LCP by a suitably designed variational principle. An "optimal" solution has been obtained in the context of the so-called "variational" procedure (VAR) [47], which was extended to polycrystals by De Botton and Ponte Castañeda [48], leading to the choice

$$\check{\tau}_{(k)}^{(r)} = 0, \quad \hat{\tau}_{(k)}^{(r)} = \left[< \tau_{(k)}^2 >^{(r)} \right]^{1/2} . \tag{17}$$

Since $\dot{e}_{(k)}^{(r)} = 0$, this procedure can be interpreted as a "generalized secant" linearization [49]. In addition, it has been shown to provide a rigourous bound for the effective potential.
More recently, the "second-order" (SO) method of Ponte Castañeda [50], extended to polycrystals in [42], has been proposed. It is based on the same variational procedure as VAR, except that the chosen LCP is not of the generalized secant type, but of a generalized affine type, not requiring the $\dot{e}_{(k)}^{(r)}$ to vanish. The reference shear stresses now read

$$\check{\tau}_{(k)}^{(r)} = \langle \tau_{(k)} \rangle^{(r)}, \quad \hat{\tau}_{(k)}^{(r)} = \check{\tau}_{(k)}^{(r)} \pm \left[< (\tau_{(k)} - \check{\tau}_{(k)}^{(r)})^2 >^{(r)} \right]^{0.5} \tag{18}$$

where the $+$ sign in the second equation has to be taken when $\check{\tau}_{(k)}^{(r)} > 0$, and the $-$ when $\check{\tau}_{(k)}^{(r)} < 0$.
The main differences between AFF, VAR, and SO models may be summarized as follows. The AFF estimate can be regarded as a relatively simple model, allowing rapid computations which can even be rather accurate for polycrystals with weak grain anisotropy and small stress sensitivity. However, its predictions can become unrealistic (*e.g.* bound violation) at strong anisotropy or nonlinearity. Contrarily to AFF for which linearization only account for the phase average stress, VAR and SO procedures account for both the phase average stress *and* intraphase standard deviation (first and second moments) to build the LCP. They can therefore provide better estimate in cases for which stress distribution is highly heterogeneous, such as for strongly nonlinear or anisotropic polycrystals. The VAR method provides a rigourous bound for the effective behavior, and can therefore improve on the AFF estimate at high anisotropy and nonlinearity. Applications of the VAR procedure to polycrystals with grains having cubic or hexagonal crystallographic structures can be found in [51, 52]. On the other hand, the SO procedure has been constructed to provide the best estimate of the effective behavior. In particular, by construction, it always complies with the VAR bound. It is therefore physically a more satisfying formulation.
Finally, the "tangent" (TGT) extension of the SC scheme [53, 54] is based on the same tangent linearization (16) as the AFF method. But, unlike the AFF extension, this procedure takes advantage of the fact that, for power law polycrystals with a single stress exponent n, the tangent behavior (14) can be replaced by a secant-like relation, with $\dot{e}_{(k)}^{(r)} = 0$ and $\alpha_{(k)}^{(r)}$ replaced by $n\alpha_{(k)}^{(r)}$. The same procedure is further applied at the macroscopic level, leading to an inconsistent definition for the stress localization tensor $\mathbf{B}^{(r)}$ that combines a secant description for the local and global behaviors but a tangent analysis for the inclusion/matrix interaction [44]. When expressed in the form of tangent expressions, it can be shown that $\dot{\bar{\varepsilon}}_0$ differs from the exact relation given in (10).

3.3 Full-field *vs.* mean-field solutions

In this section, we are showing how predictions from mean-field approaches compare to reference results obtained with full-field numerical modeling. More detailed discussions can be found *e.g.* in [55, 56].
We consider the case of a polycrystal made of grains exhibiting orthorhombic lattice symmetry, such as Olivine (a mineral from the Earth mantle), see [57, 58] for details. Grains deform by glide of dislocations on several slip planes but with only two types of Burgers vectors, parallel either to lattice directions $[100]$ or $[001]$. Since the slip plane normal $\mathbf{n}$ is normal to $\mathbf{b}$, it can be easily checked that components μ_{11}, μ_{22}, and μ_{33} of the Schmid tensors (when expressed in the crystal lattice frame) vanish. Thus, grains cannot deform axially along directions $[100]$, $[010]$, and $[001]$. In order to have adjustable grain anisotropy, we introduce another family of slip systems, namely $\{111\} < 110 >$, which allows accommodating any strain. We further define

$$M = \frac{\tau_0^{\{111\}<110>}}{\tau_0^{(010)[100]}} \tag{19}$$

where $(010)[100]$ is the softest slip system considered (*i.e.* lowest τ_0). The scalar M can be viewed as an anisotropy factor at the grain scale. A value of M close to 1 means that $\{111\} < 110 >$ exhibits a strength similar to $(010)[100]$; therefore grains can be submitted to any kind of strain-rate, *i.e.* axial deformations along directions $[100]$, $[010]$, and $[001]$ is allowed. As M increases, grain resistance increases for axial strain-rates along those directions.

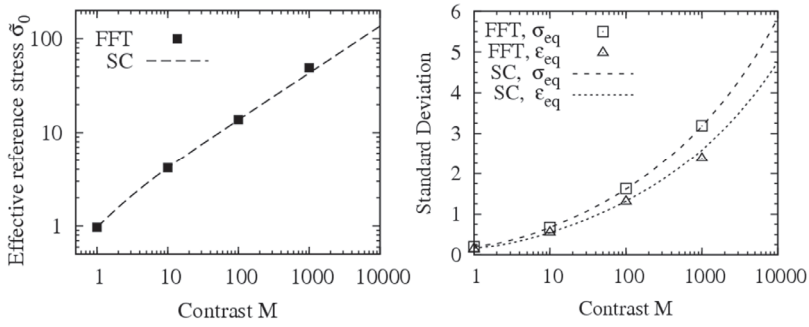

Figure 6: Full-field vs. mean-field behavior for linear isotropic orthorhombic polycrystals, as a function of the anisotropy factor M. (left) Effective polycrystal response. (right) Standard deviation of equivalent stress and strain-rate (polycrystal average). Full-field results have been generated for 50 random microstructures, and ensemble average has been performed. Mean-field results have been obtained with the SC scheme.

First of all, we consider the case of *linear viscous* behavior, corresponding to $n = 1$ in (12). In that case, the local behavior has the form (8a) with $\dot{\boldsymbol{\varepsilon}}_0 = 0$ (and $\boldsymbol{\varepsilon}$ replaced by $\dot{\boldsymbol{\varepsilon}}$ everywhere). For full-field computations, random periodic Voronoi microstructures have been considered (see figure 7a). Each of them comprises 32 grains, and ensemble average over 50 random microstructures has been performed to get good statistics. Microstructure calculation has been performed with the FFT method introduced above. Figure 6 shows how predictions from the SC scheme compare to full-field results, for both the effective flow stress and the overall standard deviation of stress and strain-rate. These standard deviations are calculated for the whole polycrystal volume, *i.e.* they account for both intragranular and intergranular heterogeneities. It can be observed that the agreement is almost perfect, even at large grain anisotropy (*i.e.* large

M). The SC scheme not only predicts the correct effective behavior, but also accurately captures the field heterogeneities within the polycrystal. Such results are in fact surprisingly good since the microstructure implicitly considered in the SC scheme is different from Voronoi tesselations; but it could indicate that microstructural details are probably not crucial for polycrystal modeling, at least in standard cases. Similar agreement have been obtained for Voronoi and EBSD 2-D microstructures under antiplane shear [23].

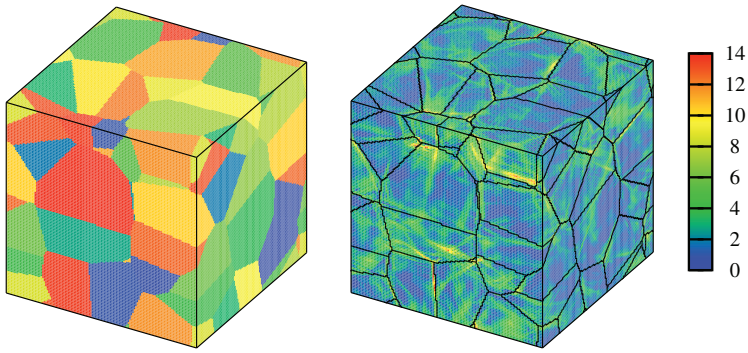

Figure 7: (left) Typical periodic random microstructure based on Voronoi tesselation, used for full-field modeling. (right) Associated field of equivalent strain-rate, normalized by the effective equivalent strain-rate, obtained for nonlinear viscoplasticity.

Figure 7 illustrates the intragranular strain-rate heterogeneity obtained in the *nonlinear* case for conditions $n = 3.5$ and $M = 100$. It can be observed that the equivalent strain-rate is highly localized, mostly (but not always) at grain boundaries; local values can exceed overall ones by more than one order of magnitude. As noted in [10, 59], local strain-rates and stresses in a given grain do depend on the grain orientation but they are also significantly influenced by the neighborhood of the grain (*i.e.* orientation, shape, and deformation of neighbor grains). Figure 8 provides the comparison between the behavior predicted by full-field and mean-field approaches. It suggests the following comments:

- As the static lower bound, the TGT linearization significantly underestimates the effective flow stress and the overall stress heterogeneities in the polycrystal. In particular, these two approaches predict a finite flow stress as $M \rightarrow \infty$, in disagreement with FFT reference results; they incorrectly predict that the polycrystal can deform without the need to activate $\{111\} < 110 >$ systems at all.

- At large M, the Taylor bound provides a flow stress proportional to M, although stress heterogeneities are underestimated. This bound significantly overestimate the activation of $\{111\} < 110 >$ at large M values.

- The AFF linearization provides a better trend, although the predicted macroscopic response is still too stiff.

- Only the SO linearization predicts accurate results, both qualitatively and quantitatively. In particular, the rapid increase of stress heterogeneities with M is correctly captured. This originates from the consideration of the first *and* second moments of the intraphase stress distribution in the definition of the LCP, which allows capturing large intraphase stress fluctuations. It means that this approach is accurately handling the mechanical interactions between grains. One important corollary is that it allows investigating effects of local deformation

mechanisms on the polycrystal behavior and field statistics. Note also that computer capacities (CPU and RAM) required by the SO model are several orders of magnitude smaller than those for the FFT.

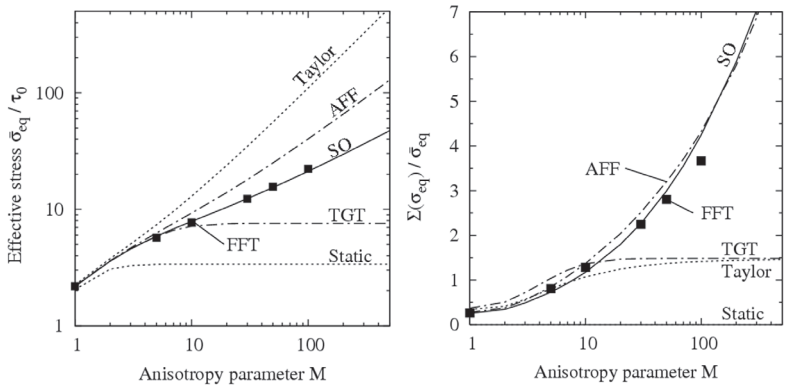

Figure 8: Full-field vs. mean-field behavior for nonlinear isotropic orthorhombic polycrystals, as a function of the anisotropy factor M. (left) Effective polycrystal response. (right) Standard deviation of the equivalent stress (polycrystal average). Mean-field results are given for various extensions of the SC scheme (AFF, SO, TGT linearizations), and for static and Taylor bounds.

4 Application to elastic thin films

We provide in this section an example of application of the above techniques to the case of elastic polycrystals with nanometric microstructures [60]. We are considering W/Cu multilayers thin films deposited on a $127.5\mu\,\mathrm{m}$ thick polyimide (Kapton) substrate. We report results for a specimen comprising 20 periods of $24\mathrm{n\,m}$ each, composed of $6\mathrm{n\,m}$ W and $18\mathrm{n\,m}$ Cu (Figure 9), for which lattice strain was investigated by X-ray diffraction during in-situ tensile tests under synchrotron radiation (see [61] for experimental details). Bragg peaks were recorded for various orientations of the diffraction vector with respect to the applied stress. Since grain size is here much smaller than the X-ray beam cross section (which is typically $100\mu\,\mathrm{m}$), and X-ray attenuation length being much larger than the specimen thickness, measurements are statistically relevant and representative of the whole specimen volume (RVE). W presents the advantage of exhibiting a high X-ray scattering factor, while Cu was chosen because of its immiscibility with W under thermodynamic equilibrium conditions. W and Cu exhibit very different elastic behaviors: at the grain scale, W is isotropic whereas Cu grains exhibit a significant anisotropy, and Young's modulus for W is globally 3 times stiffer than for Cu. The multilayer is thus a composite material with high mechanical contrast between the constituents. The structure of the specimen was carefully analyzed by several experimental techniques, showing in particular a pronounced $\{111\}$ (resp. $\{110\}$) crystallographic texture for Cu (resp. W) layers.
There are two contributions to the local elastic strain in the material. The first one is due to the localization of the applied macroscopic stress in the different grains, associated to the purely elastic response of the specimen, which is the quantity of interest here. The second contribution is associated to the residual stress generated during the elaboration process, which is not known. The advantage of performing in situ tensile tests is that once this second contribution has been characterized in the unloaded state, the purely elastic response of the specimen can be investigated,

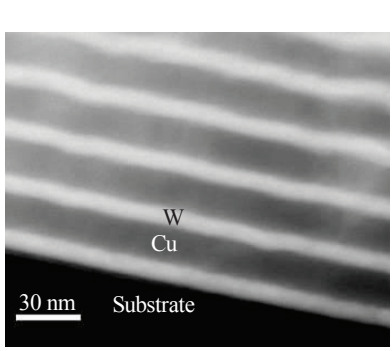

Figure 9: STEM image of a W/Cu multilayer specimen, deposited on the polyimide substrate. Respective layer thicknesses are $6\mathrm{n\,m}$ and $18\mathrm{n\,m}$. Lateral grain size is similar to layer thickness.

independently on the residual stress level and distribution. In practice, this is achieved by measuring the shift of each Bragg peak with respect to its position in the unloaded configuration [19].
Figure 10 shows the X-ray strain measurements as a function of the total applied stress for both W and Cu sublayers. The measured lattice strain is either negative or positive depending on the orientation of the diffraction vector with respect to the specimen surface and applied load direction. Strain is found to be proportional to the applied stress, indicating that deformations remain elastic, whereas the slight waviness of the data is attributed to experimental uncertainties.
To interpret these experimental results, the use of a micromechanical model is unavoidable owing to the complex microstructure of the material. Our goal is to construct a simple model that captures the main features of the material microstructure and that provides accurate and statistically relevant results. Neglecting the probable different stiffness at interfaces (grain boundaries), which may become important at very small grain sizes, three characteristic scales can be distinguished: the scale of the grain ($\mathrm{n\,m}$), the scale of the Representative Volume Element ($\mu\,\mathrm{m}$) of each layer, comprising a large number of grains, and the macroscopic scale of the specimen ($\mathrm{m\,m}$) with its laminate structure. The two last scales are related to in-plane dimensions of the film. Since the three scales differ by several orders of magnitude, the mechanical problem can be split in a first approximation into two easier scale transition problems. The first scale transition consists in evaluating the effective behavior of each (isolated) layer according to its microstructure and to the elastic behavior of grains. As discussed above, the anisotropy of the local elastic stiffness $\mathbf{C} = \mathbf{S}^{-1}$ leads to the building of mechanical interactions between grains upon macroscopic loading, resulting in heterogeneous distributions of stresses (and associated elastic strains) inside and between grains. Within W layers, the problem simplifies considerably owing to the elastic isotropy of W grains so that, from the mechanical point of view, W layers are made of a uniform isotropic material exhibiting homogeneous stress and strain, independently of the actual microstructure. The stress localization tensor $\mathbf{B}$ thus exactly reduces to identity. Concerning Cu layers, the average of $\langle \mathbf{S} : \mathbf{B} \rangle_\Omega$ has to be estimated in (4) accounting for the strong elastic anisotropy of Cu grains. Here, for sake of simplicity, we make use of the SC model although the microstructure it implicitly considers does not really match the one of individual layers (with one grain in the layer thickness). Besides its simplicity, the advantage of the SC scheme is that it allows considering the crystallographic texture for the estimation of the effective layer behavior.
The second scale transition consists of approximating the actual specimen by a laminate structure, replacing the layers containing W and Cu grains by infinite homoge-

neous layers with behavior the one predicted by the SC scheme. In doing so, the exact solution for laminate structure (*e.g.* see [62]) can be applied.
Model results are shown in Figure 10. Globally a good match to experiments is obtained, with however slightly superior results for W sublayers than for Cu. This shows that (i) the average stress level predicted for each sub-layer is accurate, and (ii) within each sublayer, the average localization of the stress in grains with different crystallographic orientations is well estimated by this simple model. It is also worth mentioning that much worse results (not shown here) are obtained when applying the Reuss bound instead of the SC scheme.

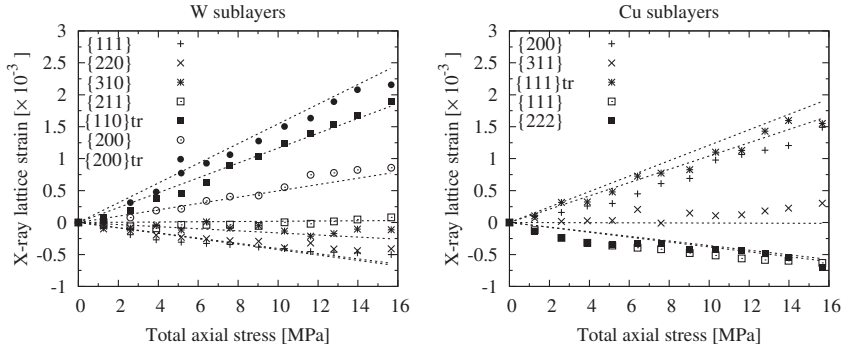

Figure 10: X-ray strain measurements (points) and elastic strain estimations based on the micromechanical SC model (dotted lines) for the sublayers versus the uniaxial stress applied to the multilayer/kapton composite. (left) W sublayers, (right) Cu sublayers.

The better results obtained for W sublayers may likely be a consequence of the larger elastic anisotropy of Cu grains as compared to W. This anisotropy renders the effective behavior of Cu sublayers sensitive to the actual microstructure, *i.e.* to crystallographic texture, grain shape and grain arrangement within the layer. Here, the real crystallographic texture of Cu sublayers could not be fully taken into account. This component shows a complex texture pattern, with dominant $\{111\}$ fiber, but other minor texture components such as probably $\{100\}$ may also be present.
One way to verify the general validity of the simple proposed model is a systematic comparison with results of a full-field scheme, as discussed above. Such calculations are reported in [60] where full-field results for a periodic composite comprising 2 layers of one grain thickness each have been obtained by the Finite Element method, and performing ensemble average over 100 random microstructures. Results have been obtained for various elastic anisotropy of Cu-like grains, and a good match to the simple mean-field solution is obtained for moderate anisotropy of the Cu layer. At least one difference between mean-field and full-field models is the estimation of field heterogeneities in each layer. By construction, the mean-field model leads to uniform stress in W layers, whereas stress heterogeneity is evidenced in the full-field approach; it comes from the heterogeneous deformation of Cu layers, associated to the elastic anisotropy of Cu grains, interacting with the homogeneous elastic W layer and generating thus some strain heterogeneities in W.
We emphasize that a more rigorous and more accurate mean-field model is still lacking at present for multilayer polycrystals. A possibility could be to make use of recent developments obtained for the homogeneization of heterogeneous plates, *e.g.* [63].

5 Conclusion

In this chapter, we have reviewed some recent experimental, theoretical, and numerical methods for the investigation of the mechanical behavior of polycrystalline materials. We have emphasized the role of strain and stress heterogeneities, which are crucial to be characterized experimentally and taken into account in the models. The use of simplistic or *ad hoc* micromechanical model should be avoided since there are many essential features for polycrystal deformation that are far from being intuitive and therefore they are not captured by such models. The topic was illustrated for elastic and viscoplastic polycrystals, but similar methods can be used for the more general case of thermo-elasto-visco-plasticity. The validity of the local constitutive relation was not discussed. For plastic deformations based of dislocation glide, it can be advantageously identified by calculations at a smaller scale *e.g.* performed by Dislocations Dynamics as detailed in a companion chapter of this volume. At nanometric sizes, the volume fraction of grain boundaries may become non-negligible compared to the volume fraction of grain interior. Since grain boundaries may exhibit a different behavior than grain interiors, this specific microstructure may be taken into account for estimating the mechanical behavior.

References

[1] R. Brenner, R.L. Lebensohn, and O. Castelnau. Elastic anisotropy and yield surface estimates. *Int. J. Solids Struct.*, 46:3018–3026, 2009.

[2] P. Feissel. *Mesures de champs et identification*, chapter 7. Du déplacement à la déformation. Hermès, 2011

[3] J. Petit, G. Montay, and M. François. Localisation phenomenon investigation on smated stainless steel samples by speckle interferometry. *Strain*, 2010.

[4] M. A. Sutton, J.S. Orteu, and H. Schreier. *Image Correlation for Shape, Motion and Deformation Measurements: Basic Concepts,Theory and Applications*. Springer, 2009.

[5] M. Bornert, J.S. Orteu, and S. Roux. *Mesures de champs et identification*, chapter 6. Corrélation d'images. Hermès, 2011.

[6] J. Réthoré, J.-P. Tinnes, S. Roux, J.-Y. Buffière, and F. Hild. Extended three-dimensional digital image correlation (x3d-dic). *C. R. Mecanique*, 336(8):643 – 649, 2008.

[7] P. Doumalin. *Microextensométrie locale par corrélation d'images numériques*. PhD thesis, Ecole Polytechnique, 2000.

[8] E. Soppa, P. Doumalin, P. Binkele, T. Wiesendanger, M. Bornert, and S. Schmauder. Experimental and numerical characterisation of in-plane deformation in two-phase materials. *Comput. Mat. Sci.*, 21:261–275, 2001.

[9] E. Héripré, M. Dexet, J. Crépin, L. Gélébart, A. Roos, M. Bornert, and D. Caldemaison. Coupling between experimental measurements and polycrystal finite element calculations for micromechanical study of metallic materials. *Int. J. Plast.*, 23:1512–1539, 2007.

[10] F. Grennerat, M. Montagnat, P. Duval, O. Castelnau, and P. Vacher. Intragranular strain field in columnar ice during transient creep. *Acta Mater.*, 2011. submitted.

[11] I.C. Noyan and J.B. Cohen. *Residual stress : measurement by diffraction and interpretation*. Springer-Verlag, 1987.

[12] C. Le Bourlot, O. Castelnau, B. Bacroix, and D. Faurie. Characterization of strain heterogeneities in polycrystals by diffraction techniques: estimation of peak moments and related uncertainties. *J. Appl. Cryst.*, 2011. submitted.

[13] G.E. Ice and R.I. Barabash. Chapter 79 white beam microdiffraction and dislocations gradients. volume 13 of *Dislocations in Solids*, pages 499 – 601. Elsevier, 2007.

[14] C. Maurice and R. Fortunier. A 3d hough transform for indexing ebsd and kossel patterns. *Journal of Microscopy-Oxford*, 230(3):520–529, 2008.

[15] A.J. Wilkinson and D. Randman. Determination of elastic strain fields and geometrically necessary dislocation distributions near nanoindents using electron back scatter diffraction. *Phil. Mag.*, 90:1159–1177, 2010.

[16] J. Villanova. *Détermination des contraintes résiduelles dans les matériaux céramiques pour SOFC : mesures multi-échelles et influence des cycles d'oxydo-réduction*. PhD thesis, Ecole Nationale Supérieure des Mines, St Etienne (France), 2010.

[17] Adam Morawiec, Raphaël Pesci, and Jean-Sebastien Lecomte. *Semiautomatic Determination of Orientations and Elastic Strain from Kossel Microdiffraction*, pages 163–169. John Wiley & Sons, Inc., 2008.

[18] N. Letouzé, R. Brenner, O. Castelnau, J-L. Béchade, and M-H. Mathon. Residual strain distribution in Zircaloy-4 measured by neutron diffraction and estimated by homogenization techniques. *Scripta Mat.*, 47:595–599, 2002.

[19] D. Faurie, O. Castelnau, R. Brenner, P.O. Renault, E. Le Bourhis, and P. Goudeau. In situ diffraction strain analysis of elastically deformed polycrystalline thin films, and micromechanical interpretation. *J. Appl. Cryst.*, 42:1073–1084, 2009.

[20] T. Ungár, O. Castelnau, G. Ribárik, M. Drakopoulos, J. L. Béchade, T. Chauveau, A. Snigirev, I. Snigireva, and B. Bacroix C. Schroer and. Grain to grain activity in cold rolled zr determined by x-ray microdiffraction line profile analysis. 55:1117–1127, 2007.

[21] M. Herbig, A. King, P. Reischig, H. Proudhon, E.M. Lauridsen, J. Marrow, J.Y. Buffière, and Ludwig W. 3-d growth of a short fatigue crack within a polycrystalline microstructure studied using combined diffraction and phase-contrast x-ray tomography. *Acta Mater.*, 59:590–601, 2011.

[22] S. Torquato. *Random Heterogeneous Materials: Microstructure and Macroscopic Properties*. Springer-Verlag, New York, 2002.

[23] R. A. Lebensohn, O. Castelnau, R. Brenner, and P. Gilormini. Study of the antiplane deformation of linear 2-d polycrystals with different microstructure. *Int. J. Solids Struct.*, 42:5441–5459, 2005.

[24] T. Kanit, S. Forest, I. Galliet, V. Mounoury, and D. Jeulin. Determination of the size of the representative volume element for random composites: statistical and numerical approach. *Int. J. Solids Struct.*, 40:3647–3679, 2003.

[25] G. B. Sarma and P. R. Dawson. Effects of interactions among crystals on the inhomogeneous deformation of polycrystals. *Acta Mater.*, 44(5):1937–1953, 1996.

[26] F. Barbe, S. Forest, and G. Cailletaud. Intergranular and intragranular behavior of polycrystalline aggregates. part 2: Results. *Int. J. Plast.*, 17:537–563, 2001.

[27] H. Resk. *Modélisation par éléments finis des hétérogénéités à l'échelle granulaire au sein d'agrégats polycristallins*. PhD thesis, Mines ParisTech, Sophia Antipolis (France), 2010.

[28] H. Moulinec and P. Suquet. A numerical method for computing the overall response of nonlinear composites with complex microstructure. *Comput. Methods Appl. Mech. Engrg.*, 157:69–94, 1998.

[29] J.-C. Michel, H. Moulinec, and P. Suquet. A computational method based on augmented lagrangians and fast fourier transforms for composites with high contrast. *Comput. Modelling Engng. Sc.*, 1:79–88, 2000.

[30] R. A. Lebensohn. N-site modeling of a 3D viscoplastic polycrystal using fast fourier transform. *Acta Mater.*, 49:2723–2737, 2001.

[31] R. A. Lebensohn, Y. Liu, and P. Ponte Castañeda. Macroscopic properties and field fluctuations in model power-law polycrystals: full-field solutions versus self-consistent estimates. *Proc. R. Soc. Lond.*, A460:1381–1405, 2004.

[32] A. Prakash and R.A. Lebensohn. Simulation of micromechanical behavior of polycrystals: finite elements vs. fast fourier transforms. *Modelling Simul. Mater. Sci. Eng.*, 17:064010, 2009.

[33] M. Bobeth and G. Diener. Static and thermoelastic field fluctuations in multiphase composites. *J. Mech. Phys. Solids*, 35:137–149, 1987.

[34] W. Kreher. Residual stresses and stored elastic energy of composites and polycrystals. *J. Mech. Phys. Solids*, 38:115–128, 1990.

[35] P. Ponte Castañeda and P. Suquet. Nonlinear composites. *Adv. Appl. Mech.*, 34:171–302, 1998.

[36] R. Brenner, O. Castelnau, and L. Badea. Mechanical field fluctuations in polycrystals estimated by homogenization techniques. *Proc. R. Soc. Lond.*, A460(2052):3589–3612, 2004.

[37] A. V. Hershey. The elasticity of an isotropic aggregate of anisotropic cubic crystals. *J. Appl. Mech.*, 21:236–240, 1954.

[38] E. Kröner. Berechnung der elastischen konstanten des vielkristalls aus den konstanten des einkristalls. *Z. Physik*, 151:504–518, 1958.

[39] J. R. Willis. Variational and related methods for the overall properties of composites. *Adv. Appl. Mech.*, 21:2–78, 1981.

[40] E. Kröner. Self-consistent scheme and graded disorder in polycrystal elasticity. *J. Phys. F: Metal Phys.*, 8:2261–2267, 1978.

[41] J. D. Eshelby. The determination of the elastic field of an ellipsoidal inclusion, and related problems. *Proc. R. Soc. Lond.*, A241:376–396, 1957.

[42] Y. Liu and P. Ponte Castañeda. Second-order theory for the effective behavior and field fluctuations in viscoplastic polycrystals. *J. Mech. Phys. Solids*, 52:467–495, 2004.

[43] P. Ponte Castañeda. Exact second-order estimates for the effective mechanical properties of nonlinear composite materials. *J. Mech. Phys. Solids*, 44:827–862, 1996.

[44] R. Masson, M. Bornert, P. Suquet, and A. Zaoui. An affine formulation for the prediction of the effective properties of nonlinear composites and polycrystals. *J. Mech. Phys. Solids*, 48:1203–1226, 2000.

[45] M. Bornert and P. Ponte Castañeda. Second-order estimates of the self-consistent type for viscoplastic polycrystals. *Proc. R. Soc. Lond.*, A454:3035–3045, 1998.

[46] M. Bornert, R. Masson, P. Ponte Castañeda, and A. Zaoui. Second-order estimates for the effective behaviour of viscoplastic polycrystalline materials. *J. Mech. Phys. Solids*, 49:2737–2764, 2001.

[47] P. Ponte Castañeda. The effective mechanical properties of nonlinear isotropic composites. *J. Mech. Phys. Solids*, 39:45–71, 1991.

[48] G. de Botton and P. Ponte Castañeda. Variational estimates for the creep behaviour of polycrystals. *Proc. R. Soc. Lond.*, A448:121–142, 1995.

[49] P. Suquet. Overall properties of nonlinear composites : a modified secant moduli theory and its link with ponte castañeda nonlinear variational procedure. *C. R. Acad. Sci. Paris*, 320(IIb):563–571, 1995.

[50] P. Ponte Castañeda. Second-order homogenization estimates for nonlinear composites incorporating field fluctuations. i – theory. *J. Mech. Phys. Solids*, 50:737–757, 2002.

[51] M. V. Nebozhyn, P. Gilormini, and P. Ponte Castañeda. Variational self-consistent estimates for cubic viscoplastic polycrystals : the effects of grain anisotropy and shape. *J. Mech. Phys. Solids*, 49:313–340, 2001.

[52] Y. Liu, P. Gilormini, and P. Ponte Castañeda. Variational self-consistent estimates for texture evolution in viscoplastic polycrystals. *Acta Mater.*, 51:5425–5437, 2003.

[53] A. Molinari, G. R. Canova, and S. Ahzi. A self-consistent approach of the large deformation polycrystal viscoplasticity. *Acta Metall.*, 35(12):2983–2994, 1987.

[54] R. A. Lebensohn and C. N. Tomé. A self-consistent anisotropic approach for the simulation of plastic deformation and texture development of polycrystals: application to zirconium alloys. *Acta Metall. Mater.*, 41(9):2611–2624, 1993.

[55] M. I. Idiart, H. Moulinec, P. Ponte Castañeda, and P. Suquet. Macroscopic behavior and field fluctuations in viscoplastic composites: Second-order estimates versus full-field simulations. *J. Mech. Phys. Solids*, 54:1029–1063, 2006.

[56] R. A. Lebensohn, P. Ponte Castañeda, R. Brenner, and O. Castelnau. Full-field vs. homogenization methods to predict microstructure-property relations for polycrystalline materials. In S. Ghosh and D. Dimiduk, editors, *Chapter 11 of Computational Methods for Microstructure-Property Relationships*, 2011.

[57] O. Castelnau, D. K. Blackman, R. A. Lebensohn, and P. Ponte Castañeda. Micromechanical modelling of the viscoplastic behavior of olivine. *J. Geophys. Res.*, 113, 2008.

[58] O. Castelnau, P. Cordier, R. A. Lebensohn, S. Merkel, and P. Raterron. Microstructures and rheology of the earth's upper mantle inferred from a multiscale approach. *C. R. Physique*, 11:304–315, 2010.

[59] O. Castelnau, R. A. Lebensohn, P. Ponte Castañeda, and D. K. Blackman. Earth mantle rheology inferred from homogenization theories. In O. Cazacu, editor, *Multi-scale modeling of heterogeneous materials*, 2008.

[60] G. Geandier, L. Gélébart, O. Castelnau, E. Le Bourhis, P.-O. Renault, and D. Thiaudière Ph. Goudeau. *IUTAM Symp. on Modelling Nanomaterials and Nanosystems*, chapter Micromechanical modeling of the Elastic Behavior of Multilayer Thin Films; Comparison with in situ data from X-Ray Diffraction, pages 99–108. IUTAM Book Series. Springer, 2009.

[61] G. Geandier, D. Thiaudière, Randriamazaoro, R. Chiron, S. Djaziri, B. Lamongie, Y. Diot, E. Le Bourhis, P. O. Renault, P. Goudeau, A. Bouaffad, O. Castelnau, D. Faurie, , and F. Hild. Development of a synchrotron biaxial tensile device for in situ characterization of thin films mechanical response. *Rev. Sci. Instrum.*, 81:103903, 2010.

[62] G. W. Milton. *The theory of composites*. Cambridge University Press, 2001.

[63] K. Bhattacharya. Thin films of active materials. In P. Ponte Castaneda, J.J. Telega, and B. Gambin, editors, *Proceedings of the NATO Advanced Research Workshop on Nonlinear Homogenization and Its Application to Composites, Polycrystals and Smart Materials*, volume 170, pages 15–44. NATO, Kluwer, 2004.